2940 0072

(115)

Item 84

Ralph J. Roberts
CENTER FOR RESEARCH
IN
ECONOMIC GEOLOGY

ANNUAL RESEARCH MEETING-1998

Program and Reports

7-8 January 1999
Midby-Byron Building
Room 107-109
University of Nevada, Reno
Reno, NV 89557

Searching Through the Carlin Time Machine

By Anthony Chakurian

CREG Annual Report
December, 1998

Introduction

Carlin was discovered in 1962. When Carlin was discovered, the deposit was the first sediment hosted disseminated gold deposit of the "Carlin Trend". The Carlin deposit has been the most studied of the sediment hosted ("Carlin" type) disseminated gold deposits. The research done at the Carlin ore body has been instrumental in understanding the "Carlin" type gold deposits. Examples of important research at Carlin include documentation of silicification and carbonate removal (Hausen and Kerr, 1968; Radtke et al., 1980; Hausen, 1985; Radtke, 1985), depth of mineralization and role of organic matter (Kuehn, 1989), and wallrock alteration associated with gold mineralization (Bakken, 1990).

The purpose of my research is to use different techniques to determine the age of gold mineralization at the Carlin deposit using samples taken from the underground workings. To be able to determine which technique would be most useful for dating gold mineralization, and to obtain well-documented samples such that the dates are meaningful requires an understanding of stratigraphy, the structural relationships, the background geochemistry of the rock units, and the geochemistry and alteration mineralogy associated with fluids travelling along faults and within permeable rock units.

Stratigraphy

Gold mineralization associated with the Carlin Underground is restricted to two stratigraphic formations: Silurian-Devonian Roberts Mountain Formation (SDrm), and Devonian Popovich Formation (Dp).

The Roberts Mountain Formation is divided into four sub-units, from top to bottom: silty limestone 1 (stls1), silty limestone 2 (stls2), silty limestone 3 (stls3), and silty limestone 4 (stls4) (Fig. 1). Each of the sub-units are informal names used by Newmont Gold in the Carlin Trend. Stls4 is the basal unit of the SDrm and comprises a thin to thickly bedded, planar laminated silty limestone. The stls3 is a thin to thickly bedded intensely bioturbated silty limestone with abundant rhythmically repeating clastic beds. Stls2 is a thin to thickly bedded, intensely bioturbated, and variably carbonaceous silty limestone. Intercalated light gray calcarenite beds are present in the upper portion of the stls2. The stls2 locally has rhythmically repeating clastic beds and debris flows with coarse sand to cobble size bioclasts. The stls1 is a thin to medium bedded, carbonaceous silty limestone with interbedded thin planar limestone and light gray calcarenite beds. The silty limestone of the stls 1 unit contains both burrows and "wispy" texture, resulting from the collapse of the burrows in intensely bioturbated areas. The thickness of stls1 varies at the top of the SDrm from 0 to 35ft due to a faulted contact. The stls1 and stls2 units of the Roberts Mountain Formation are dominantly the host of gold mineralization at Carlin. However, in the northern Carlin Trend gold mineralization dominantly occurs in the Popovich Formation, which is higher in the stratigraphic column.

Carlin Underground Stratigraphy

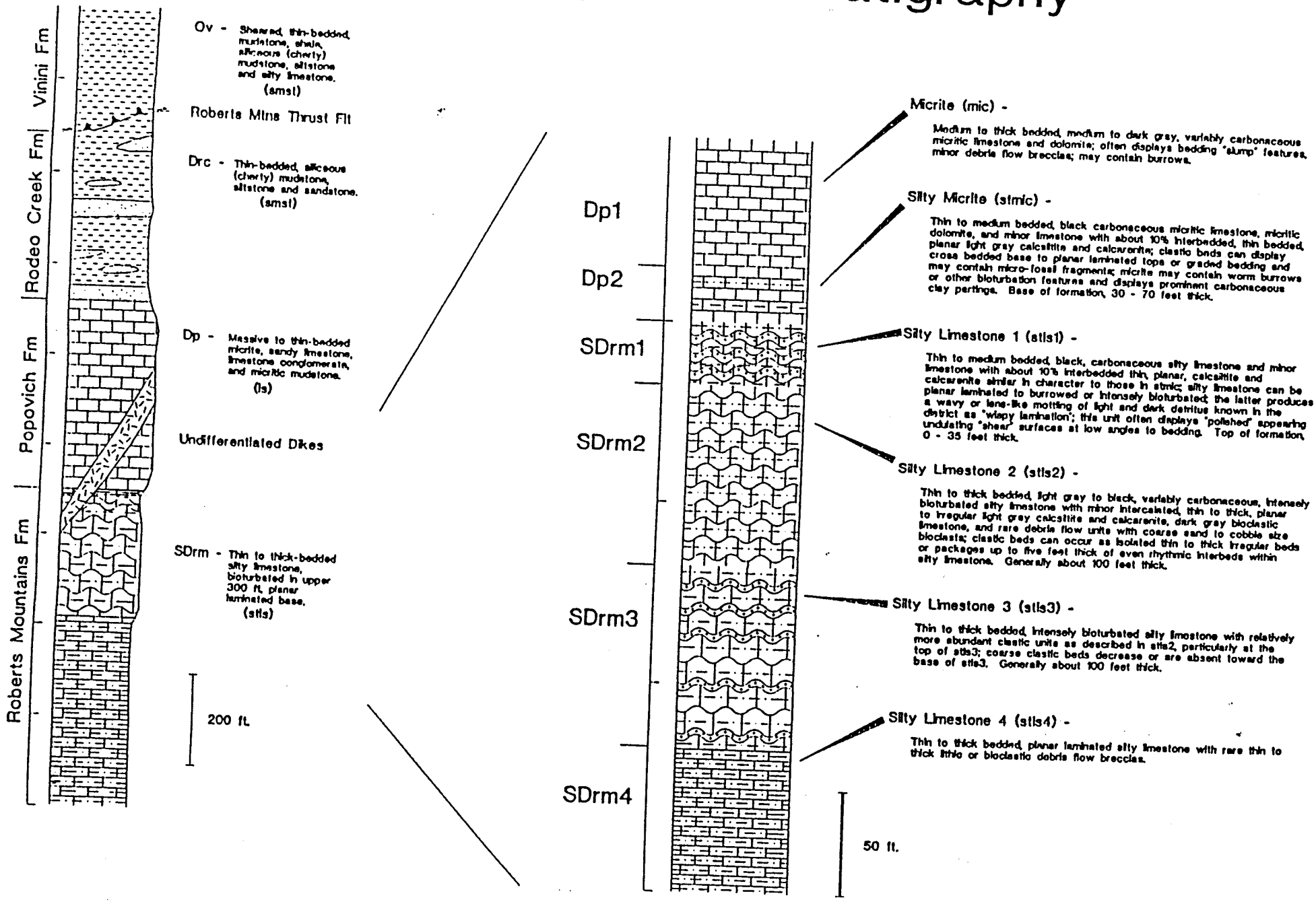

FIGURE 1. Stratigraphic Units Associated with the Carlin Underground Deposit.

The Popovich Formation overlies the SDrm and is divided into two sub-units at Carlin: micrite (Dp1), and silty micrite (Dp2) (Fig. 1). Dp2 is a thin to thickly bedded, highly carbonaceous silty micritic limestone. Dp2 is sparsely interbedded with thinly bedded light gray calcarenite beds. Dp2 is highly fractured and develops a graphitic sheen along fractures and faults. The thickness of the Dp2 unit varies between 30ft and 70ft due to the faulted contact between the stls1 and Dp2. Dp1 is a medium to thickly bedded, carbonaceous micritic limestone. Calcite veining is widespread in the Dp1 unit. Gold mineralization is sparse and localized in the Popovich Formation along large faults at Carlin.

Structure

The structural history at the Carlin deposit is complex. The deposit is in a fault block that is bounded by three regional structures: the NW bearing Castle Reef Fault, the NW bearing Leeville Fault, and the NE bearing Hardie Fault (Fig. 2). Several generations of faults and folds occur within the deposit. Igneous rocks are also exposed throughout the deposit in the form of lamprophyre dikes.

The faults present include high angle normal faults, low angle normal faults, and low angle thrust faults. The high angle normal faults are the most abundant faults associated with the Carlin deposit. Three generations of normal faults are present: NNW1 faults, NE faults, and NNW 2 faults with associated lamprophyre dikes (Table 1). The NNW1 faults are the oldest faults and are offset by the NE faults. The offset of the NNW1 faults by the NE faults are best observed by looking the Carlin Pit map that was produced by Newmont geologists. Stereonets of the exposed faults were used to identify that the structural geology of the pit is similar to the underground structures. The bearings of the NNW1 faults range from 315° to 360°.

The NE faults are the second oldest of the sets of high angle normal faults. The NE faults offset the NNW1 faults, but do not offset the NNW2 faults with the lamprophyre dikes. However, the NE faults are offset by the NNW2 faults with the lamprophyre dikes. The bearings of the NE faults range from 0° to 035°.

The NNW2 faults are the youngest of the high angle normal faults. Most of the NNW2 faults have lamprophyre dikes associated with them. The lamprophyres are primarily located along the NNW2 faults, but also occur locally where these faults with the dikes cross, large NE trending faults. The age of the lamprophyric dikes are about 158ma (McComb, 1994). The intrusion of the lamprophyric dikes at Carlin corresponds with the 158ma time of emplacement of the Goldstrike Stock (Arehart et al, 1993). The age of the lamprophyres were taken from fresh biotite grains using K-Ar dating techniques. However, some of the NNW2 do not have the associated lamprophyres. To determine whether the NNW faults without the dikes are NNW1 or NNW2, crosscutting relationships to the NE trending faults must be observed. If the fault has been offset by the NE faults, it is a NNW1 fault. If the fault has not been offset by the NE faults, it is a NNW2 fault. The orientation of the fault will not help determining whether the fault is a NNW1 or NNW2. The NNW2 faults have similar orientations to the NNW1 faults. The bearings of the NNW2 range from 330° to 360. Crosscutting relationships to NE faults are the only way to identify

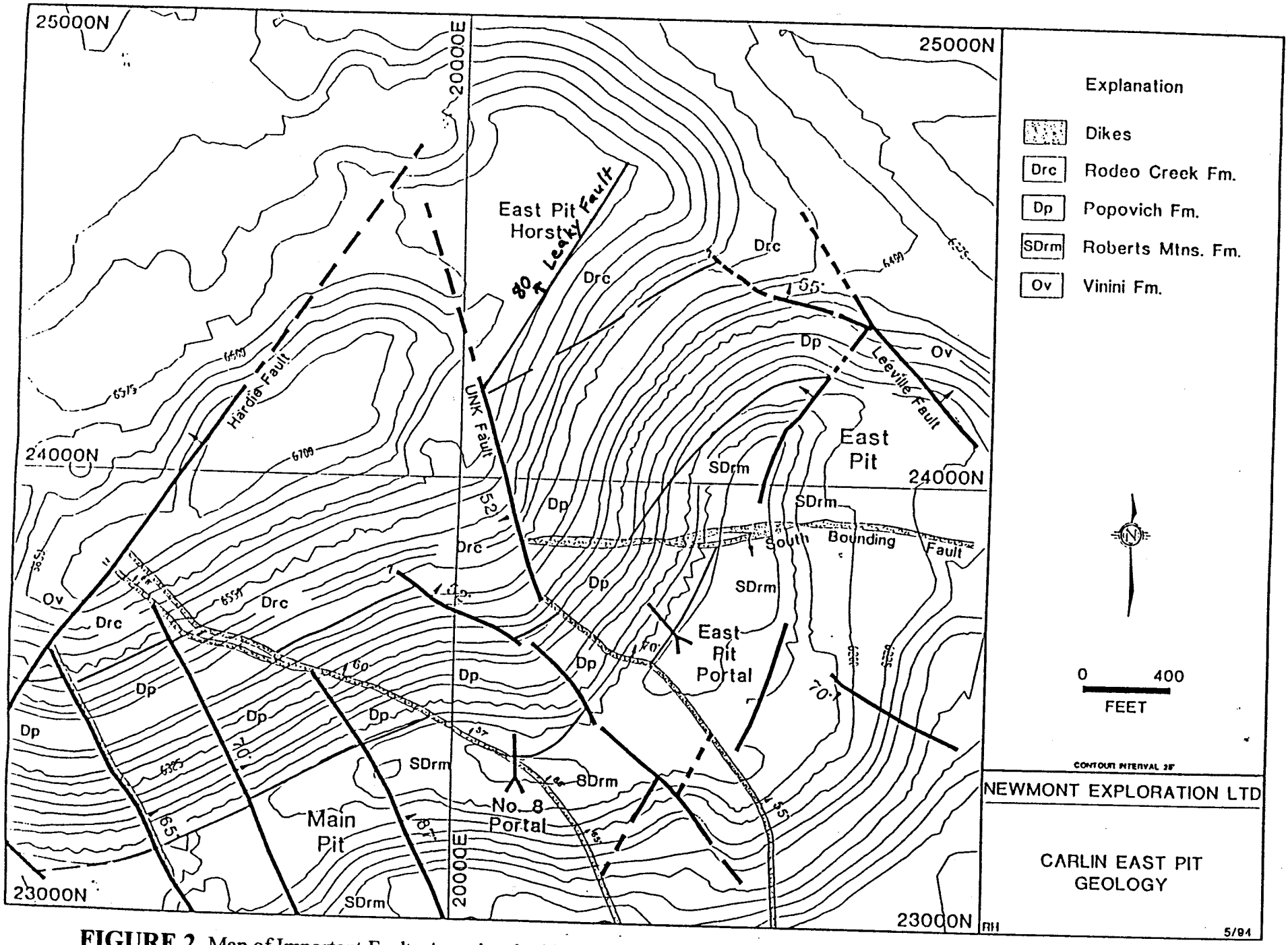

FIGURE 2. Map of Important Faults Associated with the Carlin Underground Deposit.

Carlin Structural History

Present	Oxidation
20Ma to Present	High Angle Fault Extension (Reactivation of Faults)
	Barite, Sphalerite, & Galena Veining (Remobilization)
35Ma to 20Ma	Low Angle Fault Extension (Low Angle Normal Fault Diagenesis)
	Gold Mineralizing Event
119Ma to 152Ma	Elko Orogeny (SE Dipping Thrust Faults & SW Plunging Folds)
158 Ma	Lamprophyre Dike and Goldstrike Stock Emplacement
	NNW2 Faults Develop with Strikes Ranging from 330° to 360°
	NE Faults Develop with Strikes Ranging from 0° to 035°
	Possible Development of Hardie Fault
	NNW1 Faults Develop with Strikes Ranging from 315° to 360°
360Ma to 315Ma	Antler Orogeny (Roberts Mountain Thrust, NW Dipping Thrust Faults, & NE Plunging Overturned Folds)
374Ma to 367Ma	Rodeo Creek Formation Deposited
	Sedex Barite, Sphalerite, and Galena Mineralization
394Ma to 374Ma	Popovich Formation Deposited
421Ma to 394Ma	Roberts Mountain Formation Deposited

Table 1 – Structural geologic history of the Carlin gold deposit.

if a fault without a dike is a NNW2 at Carlin. The Hardie Fault is the only NE fault that offsets NNW2 faults. However, NNW1 faults are offset by several NE faults. Even though the Hardie Fault offsets the NNW2 faults it is probably the age of the other NE faults. The offset of the NNW2 faults by the Hardie Fault is most likely due to reactivation of the NE fault by high angle fault Basin and Range Extension from 20ma to present (Thorman et al., 1991). The Hardie Fault is probably the age of the NE faults but was reactivated during Basin and Range Extension. The Hardie Fault is not younger than the NNW2 faults because of a localized presence of lamprophyric dike in the fault. The localized presence of lamprophyre in the Hardie Fault is similar to the other NE faults.

Also associated with some NNW2 faults are flower structures. The flower structures show that there has been strike slip movement along the NNW2 faults. The fault with the flower structure is a conjugate fault to the Unk Fault (Fig. 3). The Unk Fault is a NNW2 fault with a lamprophyre dike. Unfortunately, no crosscutting relationships associated with the faults bearing flower structures have been determined. More work is planned for the Unk Fault area. Because of the crosscutting relationships between the NNW1, NE, and NNW2 faults all of the high angle normal faults are pre 157ma. However, reactivation of the faults due to high angle Basin and Range Extension, have caused movement along the structures after 157ma.

Low angle faults are also present in the underground workings. Low angle thrust faults are the most prevalent. There are two sets of distinct thrust faults. One set is younger than the NNW2 faults with the lamprophyric dikes because they offset the dikes. The second set of thrust faults is probably older because they do not offset any faults or dikes and are associated with overturned folds. The oldest set of thrust faults are possibly associated with the Antler Orogeny, which occurred from 374ma to 315ma. The orientation of the thrust faults range from 053° to 096° dipping to the NW. The NW dipping thrust faults are associated with SE-verging overturned folds that plunge to the NE. The NW dipping thrust faults typically occur in the limbs of the overturned folds near the hinge. The SE-verging folds are so overturned in some places that they lay horizontally. The high degree of folding suggests that the folds have gone through multiple compressional events directed toward the SE. The lack of faults or dikes being offset by the thrust faults is an indication that thrusting occurred early in the genesis of Carlin.

The younger set of thrust faults is possibly associated with the Elko Orogeny (Thorman and others, 1990), which occurred from 152ma to 119ma. The orientation of the thrust faults range from 020° to 070° and dip to the SE. The SE dipping thrust faults are younger than the NNW2 faults because they offset the lamprophyres. The SE dipping thrust faults are younger than the dikes, but must be older than the gold mineralization event due to pooling of gold-bearing fluids along the faults.

Low angle normal faults are not as prevalent as the thrust faults but are just as important. The low angle normal faults were probably conduits for fluid flow and possibly barriers for pooling of the gold-bearing fluids. Dissolution can be found along each of the known low angle normal faults at Carlin. Only one of the three known low angle normal faults, shows gold mineralization. With only one low angle normal fault showing gold mineralization, while all of the faults show dissolution, fault development may

Simplified Cross-Section of 5550 Level Unk Fault and Conjugate Fault

SW NE

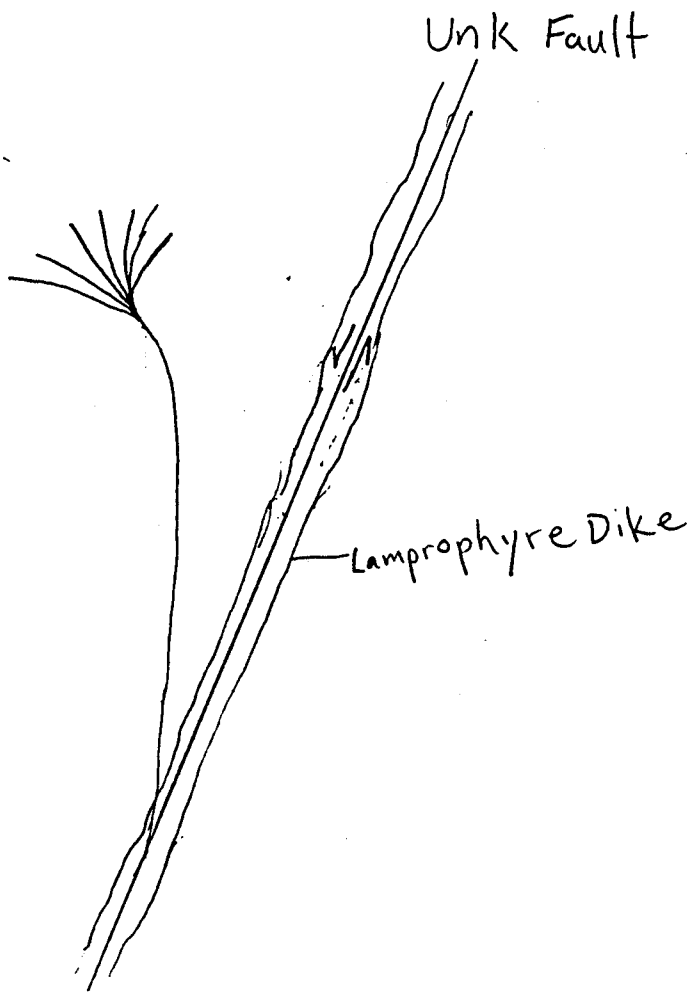

Figure 3 – Sketch of the flower structure associated with the conjugate fault of the Unk fault.

have occurred at the end of the gold mineralizing stage. The low angle normal faults are younger than the NNW2 because each one offsets a lamprophyre. However, the low angle normal faults are probably associated with a low angle detachment fault extensional event that occurred from 35ma to 20ma (Thorman et al, 1991), which was the onset of Basin and Range Extension. The orientations of the low angle normal faults vary from 020° to 066° and dip to the NW and SE. More work is planned to better understand the importance of the low angle normal faults.

Two styles of folding are present at Carlin: broad open folds and isoclinal overturned folds. The broad open folds are the prevalent throughout most of the underground workings. The open folds strike between 009° and 055° and plunge to the SW. Because the folds are open, compared to the isoclinal overturned folds, the open folds probably experienced one compressional event. The SE dipping thrust faults may be associated with the open folds. Of the two folding events the one associated with the open folds is youngest and may be associated with the Elko Orogeny.

The isoclinal overturned folds are localized around the Hardie Fault. The folds strike between 028° and 078°, plunge to the NE, and show SE vergence. The isoclinal folds are associated with the NW dipping low angle thrust faults. The isoclinal folds have seen intense compression from the NE overturning the axis of the folds up to 90° locally. The degree of overturning suggests that folds have undergone intense compression and probably multiple contractional events. The exposure of the folds to multiple events suggests that diagenesis occurred during the Antler Orogeny. The high degree of compression in such a localized area may have resulted in the development of the Hardie Fault as a reverse fault, prior to later normal displacement. Similar reverse displacements have been described at Betze-Post along NNW striking faults on the western limb of the Post anticline (Leonardson and Rahn, 1996).

Gold mineralization at Carlin is predominantly controlled by NE faults. These NE faults are the primary conduits that the gold-bearing fluids travel along. The NE faults are not the only fluid conduits. Some of the NNW2 faults control fluid flow. From the conduits the gold-bearing fluids permeate into host strata. Areas with low angle thrust faults typically show higher gold grades associated with the pooling of gold-bearing fluids along the structures. Along all low angle normal faults dissolution is present. Some of the low angle normal faults show gold mineralization resulting from the fluid flow along the faults. As previously observed, the structures at Carlin are an important control of the movement and deposition of the gold bearing fluids.

Geochemistry

To better understand the main and late stage gold bearing fluids it is important to first understand the geochemistry of each of the stratigraphic rock units. Newmont Gold's trace element geochemistry of the NW orebody at Carlin was used to examine differences in the stratigraphic rock units. The samples used for the geochemistry were processed and analyzed by Chemex Labs, Inc. The samples sent were parts of drill core. To determine the stratigraphic units of the cores that were analyzed, the samples were correlated with their core logs. The geochemical results selected were based on whether the samples had

one or multiple stratigraphic units. Only the geochemical results from samples with one stratigraphic unit was used. The selection of samples with only a single stratigraphic unit attempts to decrease the possibility of error due to dilution or enhancement of elements by other rock units. After collecting and separating the data, the average geochemistry of each of the stratigraphic units was determined. The rock unit averages were then compared to Clark crustal geochemical averages for limestones and black shales, and background levels for the SDrm and Dp (Radtke, 1985). The tables produced were separated into major oxide (Table 2A) and trace element geochemistry (Table 2B). The stratigraphic unit averages show that gold mineralization is predominantly in the SDrm 1 and SDrm 2. Analysis of the geochemistry of each sample verifies that gold mineralization is primarily hosted in the SDrm 1 and SDrm 2 (Fig. 4). Correlation of the geochemical results (Table 3) shows that Ag, Cd, Cu, Mo, Ni, V, and Zn are related to each other. Values for Ag, Cd, Cu, Mo, Ni, V, and Zn are elevated in the Dp2 compared to the other stratigraphic units. The Dp2 also shows elevation in the carbon content compared to the other stratigraphic units. The elevated values of the Ag, Cd, Cu, Mo, Ni, V, and Zn may be associated with the high carbon content of the Dp2 unit. The Dp2 may be similar to a black shale in its composition due to its high carbon content and the elevated levels of base metals.

Leaky Fault System

Understanding the geochemistry and the alteration mineralogy of the fluids traveling along the structures and stratigraphic units is essential in determining what phases might be able to give a date that corresponds to the gold mineralizing event. With gold mineralization typically associated with silicification, highly silicified zones would be best for looking at the geochemistry of gold-bearing fluids. Through most of the Carlin underground, there are not many localities that are highly silicified. The areas that are the most silicified are along faults. The Leaky Fault system in the 5720 level is the most silicified locality in the Carlin underground. Along a traverse across the Leaky Fault system, nine samples were taken at intervals of 2ft. The samples include the main Leaky Fault and two conjugate faults. Sample TCCA 48 is from the main Leaky Fault with TCCA 50, and 57 from conjugate faults (Fig. 5). TCCA 50 is the conjugate fault in the footwall of the Leaky Fault, while TCCA 57 is the conjugate in the hanging wall. Along the main Leaky Fault and its hanging wall to the NW, values for Ba, Zn, Sr, V, and Cu are elevated (Fig. 6). The elevated values are associated with barite and sphalerite veining along the Leaky Fault. X-ray diffraction of samples taken from the traverse shows a trace mineral alteration halo associated with the barite and sphalerite veining. Between the Leaky Fault and the hanging wall conjugate fault vanadian, barian, and magnesian muscovite is present. Extending from the Leaky Fault to the footwall conjugate fault, the vanadian, barian, and magnesian muscovite changes to illite-montmorillonite. The change from muscovite to illite-montmorillonite is probably a proximal to a distal relationship along the fault system. Petrographic work on the nine samples from the Leaky Fault system shows that the barite is overprinting

Carlin Underground Average Major Oxide Geochemistry

Rock Unit	# of Samples	Carbon Level	Al (%)	Ca (%)	Fe (%)	K (%)	Mg (%)	Na (%)	Ti (%)
DP 1	11	High	2.92	20.5	1.42	1.36	3.8	0.04	0.16
DP 2	9	Very High	1.86	15.4	1.27	0.8	5.16	0.02	0.09
SDRM 1	100	High	3.2	9.16	1.74	1.46	4.46	0.03	0.16
SDRM 2	146	Moderate	3.66	7.85	1.71	1.53	4.35	0.04	0.19
SDRM 2 Internal Stls 1	16	Moderate	3.35	6.71	1.58	1.44	3.96	0.03	0.17
Dike Material	9	Low	7	2.8	5.55	1.75	1.06	0.14	0.93
Dike & Sed Material	10	Low	4.97	5.63	2.74	1.76	3.11	0.09	0.33
Detection Limits	N/A	N/A	0.01	0.01	0.01	0.01	0.01	0.01	0.01
Clark Limestone Values	N/A	N/A	N/A	N/A	1.3	0.27	N/A	N/A	0.4
Clark Black Shale Values	N/A	N/A	N/A	N/A	N/A	N/A	N/A	N/A	N/A
SDRM Background Levels	N/A	N/A	0.72	47.8	0.6	0.13	0.61	0	0.09
DP Background Levels	N/A	N/A	0.2	50.1	0.44	0.09	2.3	0.02	0

Carbon Level

Very High: High Amounts of Visible Organic Material in Thin Sections
High: Visible Organic Material in Thin Sections
Moderate: Sooty Color of Samples
Low: Lack of Sooty Color of Samples

Table 2-A - Average Major Oxide Geochemistry of the Stratigraphic Units in the Carlin Underground with comparisons to Clark Crustal Values for Limestones and Black Shales

Carlin Underground Average Trace Element Geochemistry

Rock Unit	# of Samples	Carbon Level	Au (ppb)	As (ppm)	Sb (ppm)	Hg (ppb)	Ag (ppm)	Ba (ppm)	Be (ppm)	Bi (ppm)	Cd (ppm)	Co (ppm)
DP 1	11	High	380	44	6.5	1304	0.2	620	0.8	4	0.6	5.6
DP 2	9	Very High	526	54	6.9	4967	0.3	307	0.5	2.4	4.8	2
SDRM 1	100	High	5659	362	53	14903	0.2	338	0.6	2.7	1.3	5.4
SDRM 2	146	Moderate	2198	356	57	5127	0.2	431	0.7	2.8	0.7	6
SDRM 2 Internal Stls 1	16	Moderate	1279	331	124	4738	0.2	333	0.7	2.5	0.7	5.4
Dike Material	9	Low	N/A	1656	83	18080	0.2	14	0.8	2.9	1.3	27
Dike & Sed Material	10	Low	4050	1096	74	8877	0.2	165	0.9	3.2	0.8	13
Detection Limits	N/A	N/A	N/A	1	0.2	10	0.2	10	0.5	2	0.5	1
Clark Limestone Values	N/A	N/A	5	1.1	0.3	40	0.2	92	<1	0	0.035	0.1
Clark Black Shale Values	N/A	N/A	10	75	0	N/A	5	450	1	0	0	5
			Au (ppm)			Hg (ppm)						
SDRM Background Levels	N/A	N/A	<.03	<5	0.5	6	N/A	30	<1	N/A	N/A	<2
DP Background Levels	N/A	N/A	N/A	<1	<.3	N/A	N/A	50	<1	N/A	N/A	<2

Carbon Level

Very High: High Amounts of Visible Organic Material in Thin Sections
High: Visible Organic Material in Thin Sections
Moderate: Sooty Color of Samples
Low: Lack of Sooty Color of Samples

Table 2-B - Average Trace Element Geochemistry of the Stratigraphic Units in the Carlin Underground with comparions to Clark Crustal Values For Limestones and Black Shales.

Cr (ppm)	Cu (ppm)	Mn (ppm)	Mo (ppm)	Ni (ppm)	P (ppm)	Pb (ppm)	Sr (ppm)	V (ppm)	W (ppm)	Zn (ppm)
58	14	212	2	18	306	9	263	51	10	39
44	49	171	38.1	71	470	11	168	390	10	285
52	25	188	8	30	582	10	104	112	10	100
53	22	199	5	25	470	12	67	76	10	50
51	19	174	4.8	24	493	11	66	76	10	69
47	37	172	4.3	36	1664	63	84	192	34	97
53	24	251	5.8	46	742	19	94	108	13	73
1	1	5	1	1	10	2	1	1	10	2
11	5	1100	0.4	20	400	5	610	20	1.8	21
10	20	N/A	10	20	N/A	20	N/A	50	N/A	100
					P (%)					
10	1.5	200	N/A	2	0.06	N/A	700	7	N/A	<6
7	2	50	N/A	<1	0.05	N/A	200	7	N/A	25

Figure 4 - Gold geochemistry of the different stratgraphic units in the Carlin deposit

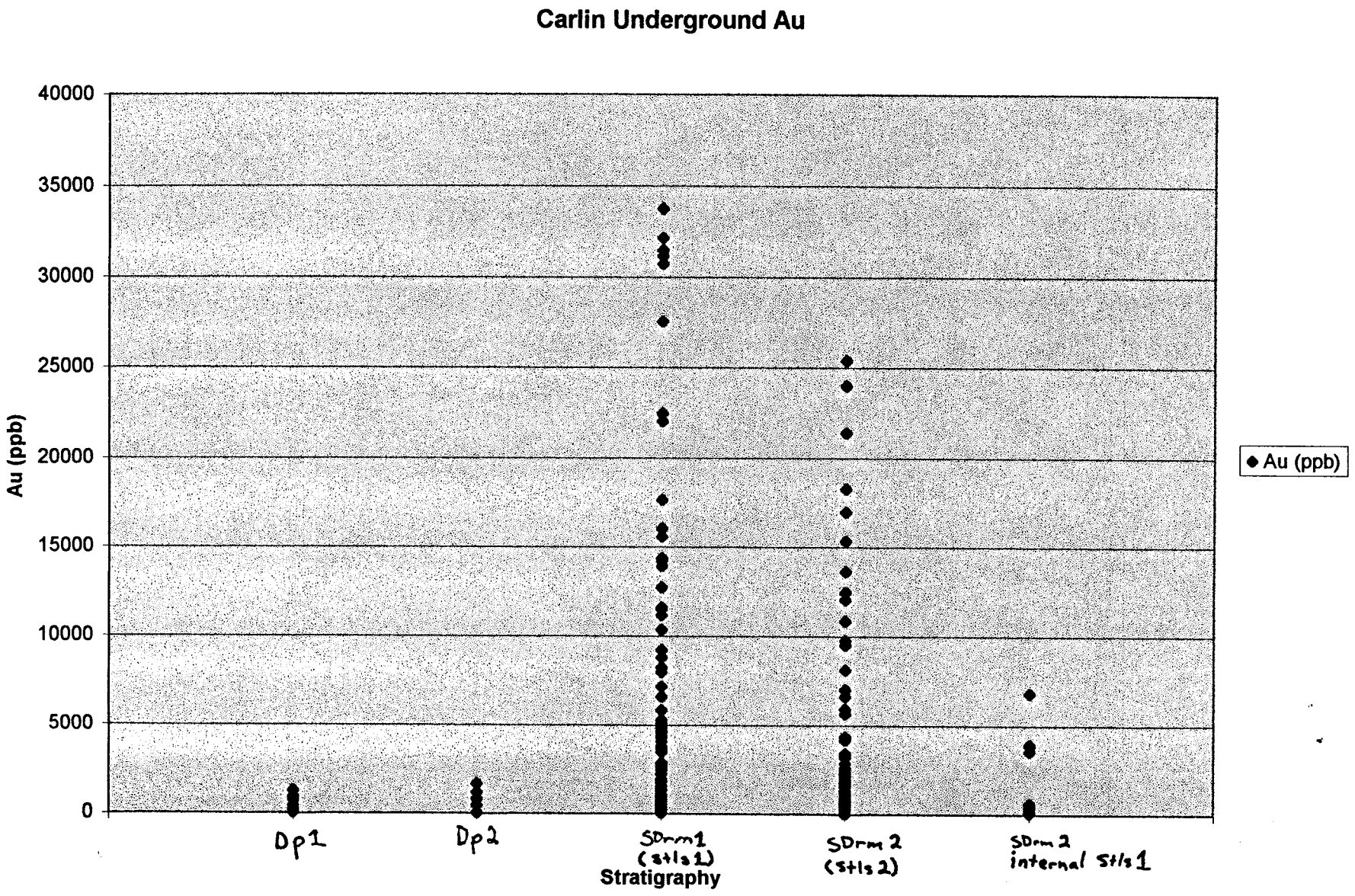

Anthony Chakurian, CREG 1998 Annual Report

Table 3 - Correlation values of the stratigraphic unit geochemistry averages at the Carlin deposit.

	Au	*As*	*Sb*	*Hg*	*Ag*	*Al*	*Ba*	*Be*	*Bi*	*Ca*	*Cd*	*Co*	*Cr*	*Cu*	*Fe*	*K*	*Mg*	*Mn*	*Mo*	*Na*	*Ni*	*P*	*Pb*	*Sr*	*Ti*	*V*	*Zn*
Au (ppb)	1																										
As (ppm)	**0.6965**	1																									
Sb (ppm)	0.22303	**0.76769**	1																								
Hg (ppb)	**0.9587**	0.59045	0.17924	1																							
Ag (ppm)	-0.3828	-0.5938	-0.4941	-0.1357	1																						
Al (%)	0.40511	**0.79089**	0.6298	0.16432	**-0.9221**	1																					
Ba (ppm)	-0.3519	-0.4188	-0.4226	-0.5466	-0.4294	0.2059	1																				
Be (ppm)	-0.2344	0.04355	0.17597	-0.4769	**-0.7845**	0.63433	**0.81758**	1																			
Bi (ppm)	-0.2696	-0.4597	-0.4601	-0.4405	-0.4155	0.13231	**0.97877**	**0.76738**	1																		
Ca (%)	-0.5165	**-0.9341**	**-0.8383**	-0.4874	0.33196	-0.6014	0.65012	0.16437	**0.71042**	1																	
Cd (ppm)	-0.2391	-0.5226	-0.4851	0.01686	**0.98805**	**-0.9137**	-0.5047	**-0.8604**	-0.4708	0.27859	1																
Co (ppm)	0.34241	0.59056	0.44834	0.07777	**-0.9886**	**0.94583**	0.47011	**0.80247**	0.42982	-0.3291	**-0.9871**	1															
Cr (ppm)	0.06906	0.09505	0.01626	-0.1858	**-0.8447**	0.64446	**0.83993**	**0.92415**	**0.83588**	0.21048	**-0.8719**	**0.8534**	1														
Cu (ppm)	-0.1178	-0.352	-0.389	0.13035	**0.95429**	**-0.8146**	-0.6244	**-0.9261**	-0.6073	0.10243	**0.9797**	**-0.9434**	**-0.9267**	1													
Fe (%)	**0.77285**	**0.92797**	0.56497	0.59603	**-0.7714**	**0.88254**	-0.1098	0.25176	-0.1357	**-0.7359**	**-0.6952**	**0.7781**	0.39498	-0.549	1												
K (%)	0.45638	**0.72226**	0.55147	0.2088	**-0.9788**	**0.97763**	0.30885	0.69373	0.27063	-0.4811	**-0.9595**	**0.9643**	**0.75368**	**-0.8868**	**0.86876**	1											
Mg (%)	0.08303	-0.1862	-0.3872	0.29741	**0.8589**	-0.6798	-0.649	**-0.9469**	-0.6404	-0.0139	**0.90759**	**-0.8329**	**-0.8817**	**0.96686**	-0.3475	**-0.7571**	1										
Mn (ppm)	-0.0107	-0.1321	-0.3834	-0.2504	-0.5796	0.41852	**0.91901**	**0.76125**	**0.89035**	0.43517	-0.6134	0.6374	**0.88769**	-0.6689	0.22031	0.51382	-0.5908	1									
Mo (ppm)	-0.2551	-0.4925	-0.4452	6.7E-05	**0.9899**	**-0.8927**	-0.5323	**-0.8644**	-0.5096	0.23407	**0.99779**	**-0.9844**	**-0.8942**	**0.98543**	-0.6823	**-0.9519**	**0.91376**	-0.6401	1								
Na (%)	0.00602	0.21099	0.04416	-0.2773	**-0.8018**	**0.74578**	**0.78568**	**0.89104**	**0.70334**	0.05237	**-0.8503**	**0.8661**	**0.91485**	**-0.8531**	0.47552	**0.77975**	**-0.7648**	**0.89119**	**-0.8515**	1							
Ni (ppm)	-0.2046	-0.4406	-0.417	0.05087	**0.97982**	**-0.8685**	-0.5748	**-0.8919**	-0.5523	0.18266	**0.99466**	**-0.9744**	**-0.9126**	**0.99366**	-0.6368	**-0.932**	**0.93374**	-0.6623	**0.99813**	**-0.8626**	1						
P (ppm)	**0.76314**	**0.72235**	0.4764	**0.8552**	0.0325	0.15806	**-0.8651**	-0.6322	**-0.825**	**-0.7861**	0.15362	-0.0737	-0.5075	0.31151	0.54419	0.10015	0.442	-0.6183	0.16973	-0.4739	0.22721	1					
Pb (ppm)	-0.0207	0.48439	0.40946	0.00136	0.19612	0.19577	-0.5718	-0.3462	**-0.7266**	-0.6916	0.17549	-0.1131	-0.5144	0.33235	0.24072	-0.0104	0.40642	-0.4521	0.23659	-0.1572	0.26923	0.4493	1				
Sr (ppm)	-0.4614	**-0.8942**	**-0.7885**	-0.4477	0.23063	-0.535	0.68927	0.2372	**0.765**	**0.99111**	0.18388	-0.2413	0.29936	0.00168	-0.6759	-0.3948	-0.1143	0.47762	0.13517	0.10178	0.08378	**-0.7843**	**-0.7779**	1			
Ti (%)	0.312	0.68429	0.54228	0.05139	**-0.9461**	**0.98734**	0.35892	**0.74218**	0.28051	-0.4717	**-0.9532**	**0.9759**	**0.74655**	**-0.8785**	**0.81636**	**0.97969**	**-0.7577**	0.54069	**-0.9365**	**0.83758**	**-0.9208**	0.00371	0.10437	-0.4029	1		
V (ppm)	-0.2405	-0.4907	-0.4483	0.01597	**0.98802**	**-0.8953**	-0.5356	**-0.87**	-0.5089	0.23572	**0.99863**	**-0.9846**	**-0.8933**	**0.98594**	-0.6781	**-0.9513**	**0.91558**	-0.6407	**0.99979**	**-0.8569**	**0.99829**	0.1782	0.22412	0.13836	**-0.9399**	1	
Zn (ppm)	-0.1845	-0.4577	-0.4069	0.08169	**0.97356**	**-0.8936**	-0.5824	**-0.8958**	-0.5402	0.20462	**0.99465**	**-0.9834**	**-0.9067**	**0.983**	-0.6531	**-0.9409**	**0.91155**	-0.6843	**0.99374**	**-0.8986**	**0.99458**	0.23607	0.1931	0.11533	**-0.9465**	**0.995**	1

SE

NW

5720 Level Leaky Fault System

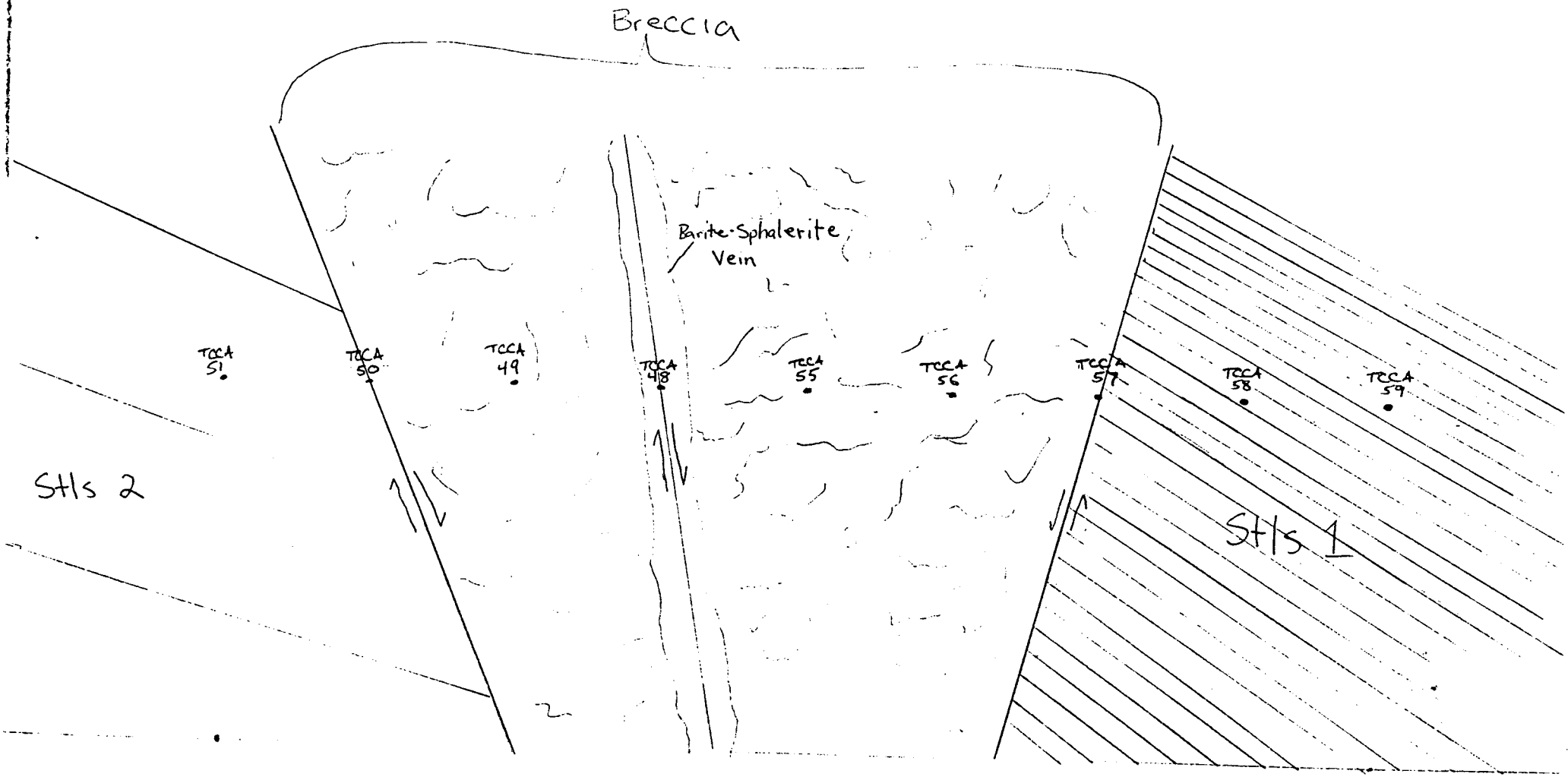

Figure 5 – Rib sketch of the Leaky Fault system in the 5720 Level of the Carlin Underground.

0 2ft

1 in = 2ft

Author: C. Clark

Figure 6 - Graph showing elevation of values for Ba, Su, Sr, V, and Zn due to fluid flow along the Leaky Fault

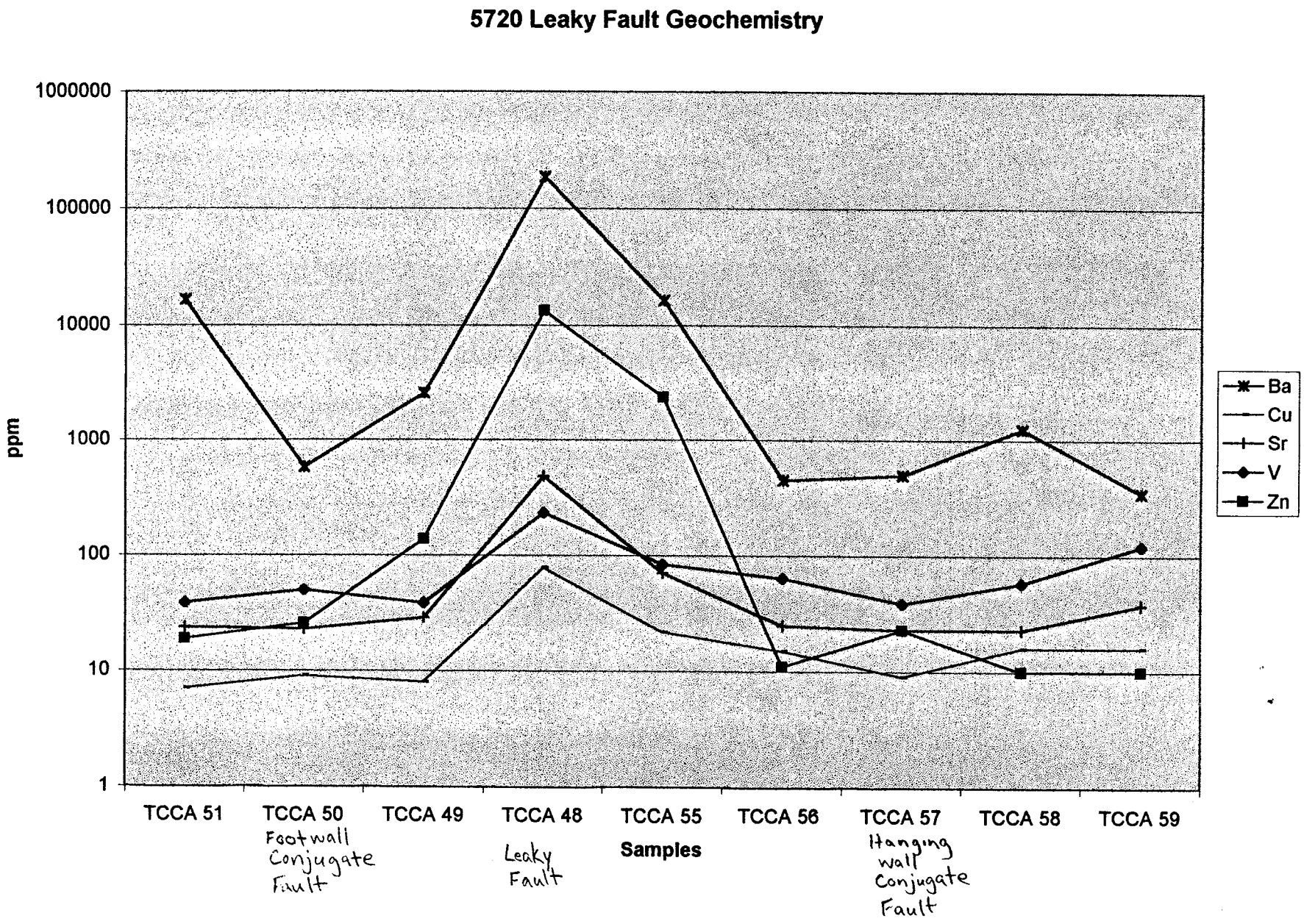

AnthonyChakurian, CREG 1998 Annual Report

the silicification event (Fig. 7). The overprinting of the barite on top of the quartz shows that the veining and associated alteration assemblage is probably from late non-gold bearing fluids.

Potential Dating Techniques That May Be Used

Determining the time of the gold mineralizing events of the Carlin-type deposits has been difficult in the past due to the lack of datable material. This research project is attempting to determine the age of gold mineralization using samples carefully selected so that the paragenetic relationship between the sample and gold mineralization is well documented. During this research multiple dating techniques will be attempted. Techniques that will most likely be used will be: Ar^{40}/Ar^{39} of sericite grains in lamprophyric dikes with high gold grades, fission track dating of zircons in highly mineralized zones, U-Pb dating of hydrothermal apatite, and rhenium-osmium dating of realgar. However, other dating techniques may also be used as research continues.

Potentially the most intriguing results will come from the Ar^{40}/Ar^{39} dating of the sericite grains in the lamprophyric dikes. Dating of sericites from lamprophyres in Carlin-type deposits previously have given inconsistent results due to not clearly tying the samples to the mineralizing event (Kuehn, 1989; McComb, 1994). The inconsistent results of the sericite dating are due to using lamprophyric samples with minimal gold mineralization. The low gold levels in the lamprophyres means that the time for completely resetting or generation of new sericite grains by the gold-bearing fluids was minimal. The partially reset or composite sericite grains would then give dates older than the true gold mineralizing event. The lamprophyric dike to be used from Carlin is different from most of the other dikes. The 8-A dike, unlike other lamprophyres in Carlin, contains high-grade mineralization. The gold grade varies from the hanging wall of the 8-A dike to the footwall. The hanging wall of the dike has a gold grade of .1730 opt. The grade of gold for the internal portion of the dike is .1392 opt. The highest gold grades in the 8-A dike occur in the footwall with a value at .6260 opt (fig. 8). The wallrock surrounding the 8-A dike has gold grades of .0X opt. Samples containing sericite grains next to pyrite grains with arsenian rims will be used for dating. Arsenic scans on the SEM will be used to determine whether the pyrite grain has arsenian rims. The Ar^{40}/Ar^{39} dating of the sericite in the 8-A dike could potentially produce the best results of the study.

Fission track dating of zircons will also be used in the study. The fission track dating will be used in areas that have seen a high degree of fluid flow. The assumption being that the heat from the fluids will reset the fission track clock of the zircon. Two localities for samples have been selected. The first locality selected contains high-grade gold ore with grades of .7256 opt. The second area selected is highly silicified but lower gold grade. The assumption is that the large quantity of fluids that traveled through the selected localities reset the zircons to the date of gold mineralization.

U-Pb dating will be used on hydrothermal apatites. Hydrothermal apatite is present in the silicified zones in Carlin. The idea of U-Pb dating is that the hydrothermal apatites have an original amount of Pb that can only be increased by radiogenic decay of the uranium. However it is important to determine, prior to dating the common Pb correction. Without a common Pb correction the results of the

TCCA 55 Thin Section

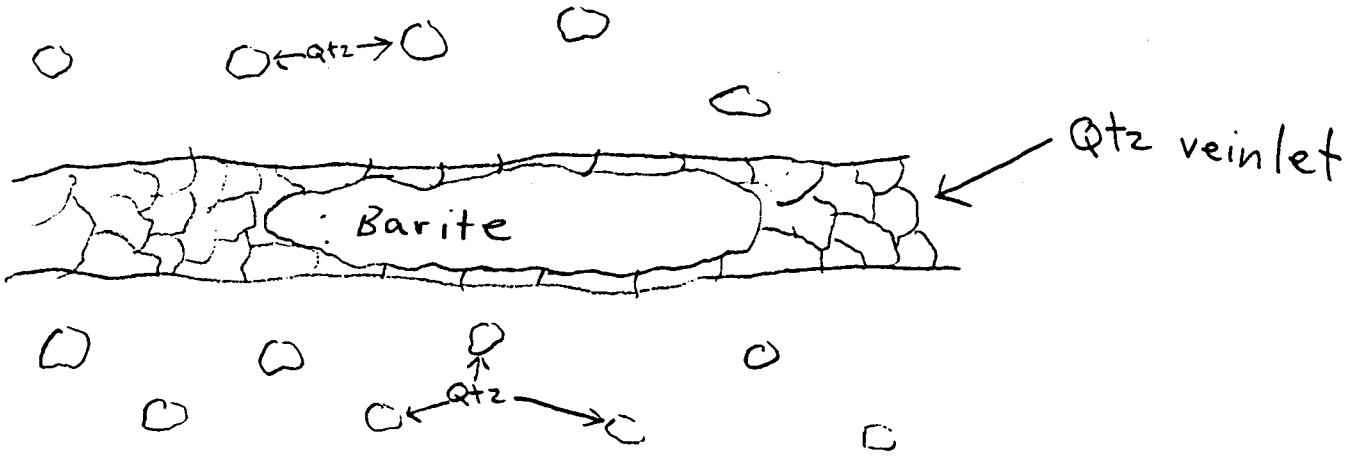

Figure 7 – Sketch of thin section TCCA 55 showing barite mineralization post dating quartz mineralization

SE

NW

5860 Carlin Main 8-A Dike

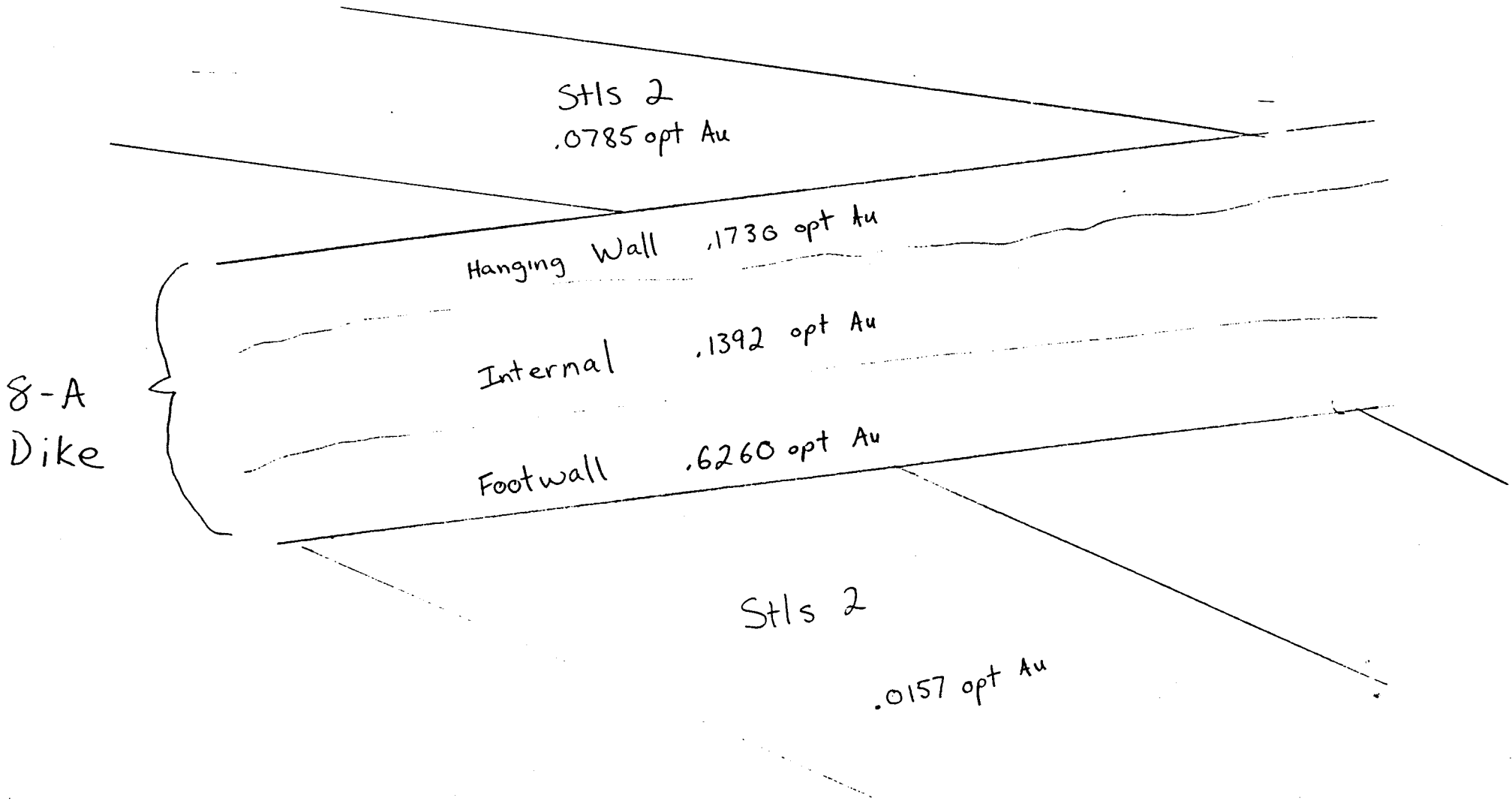

Figure 8 – Rib sketch and gold assay values for the 8-A dike and wallrock in the 5860 Level of the Carlin Main Underground

0 1in=1ft 1ft

dating could be skewed background lead values. For this study the Pb correction will be determined by other minerals that are associated with mineralization such as: realgar and stibnite. At the present, suitable samples containing hydrothermal apatite have not been selected.

Rhenium-osmium dating will be attempted on realgar to see what type of results will be produced. The realgar dating technique will be compared with dates produced by other methods to determine how effective the process is. At present, samples are in for testing at the lab of Joaquin Ruiz at the University of Arizona.

Another potential way to determine the age of the mineralizing event is to look at the low angle normal faults. The alteration assemblage associated with the dissolution along the low angle normal faults may present more opportunities for dating mineralization. Elevated gold values must be observed along the low angle normal faults used for the research. The elevated values would tie the fluid flow along the fault with gold mineralization.

As the research continues more possible dating techniques may be observed as useable for dating the gold mineralizing event at Carlin.

Conclusion

Understanding of the geology and structural history of the Carlin deposit is important in determining the age of gold mineralization. Previous attempts to constrain the date of mineralization have had limited success due to not correlating and documenting the relationship between the samples used and the gold mineralizing event. The time of mineralization at Carlin can be dated but the samples must be linked paragenetically to mineralization to give proper constraint to the results.

References Cited

Arehart, G. B., Foland, K. A., Naeser, C. W., and Kesler, S. E., 1993, $^{40}Ar/^{39}Ar$, K/Ar, and Fission Track Geochronology of Sediment-Hosted Disseminated Gold Deposits at Post-Betze, Carlin Trend, Northeastern Nevada: Economic Geology, v. 88, p. 622-643

Bakken, B. M., 1990, Gold Mineralization, Wall-Rock Alteration, and the Geochemical Evolution of the Hydrothermal System in the Main Orebody, Carlin Mine: UMI Dissertation Services, 236 p.

Carlin Underground Mine Geology Staff, 1995, The Carlin Underground Project: NEL Annual Meeting, Newmont Exploration Limited

Harris, R. H., 1996, Carlin Underground Gold Deposits, Newmont Exploration Limited

Hawkes, H. E., and Webb, J. S., 1962, Geochemistry In Mineral Exploration, Harper & Row, Publishers, New York and Evanston, 415 p.

Kuehn, C. A., 1989, Studies of Disseminated Gold Deposits Near Carlin, Nevada: Evidence for a Deep Geologic Setting of Ore Formation: UMI Dissertation Services, 396 p.

Leonardson, R. W., and Rahn, J. E., Geology of the Betze-Post gold deposits, Eureka County, Nevada: Geology and Ore Deposits of the American Cordillera: Geological Society of Nevada Syposium Proceedings, Reno/Sparks, Nevada, April 1995, p. 61-94

McComb, M. B., 1995, Petrographic Examination and Semiquantitative XRD-XRF Analysis of Dike Rocks From Carlin Underground, Newmont Exploration Limited Metallurgical Services

Radtke, A. S., 1985, Geology of the Carlin Gold Deposit, Nevada: U.S. Geological Survey Professional Paper 1267, 124 p.

Thorman, C. H., Ketner, K. B., and Peterson, Fred, 1990, The Elko orogeny – Late Jurassic orogenesis in the Cordilleran miogeocline: Geological Society of America, Cordilleran Section Meeting, Tuscon, Arizona, v. 22, number 3, p. 88

Thorman, C. H., Ketner, K. B., Brooks, W. E., Snee, L. W., and Zimmermann, R. A., 1991, Late Mesozoic-Cenozoic Tectonics in Northeastern Nevada: Geology and Ore Deposits of the Great Basin, Symposium Proceedings, v. 1, p. 25-45